Spectroscopic Signatures of Quantum Many-Body Correlations in Polariton Microcavities

Jesper Levinsen,[1,2] Francesca Maria Marchetti,[3] Jonathan Keeling,[4] and Meera M. Parish[1,2]
[1]School of Physics and Astronomy, Monash University, Victoria 3800, Australia
[2]ARC Centre of Excellence in Future Low-Energy Electronics Technologies, Monash University, Victoria 3800, Australia
[3]Departamento de Física Teórica de la Materia Condensada & Condensed Matter Physics Center (IFIMAC), Universidad Autónoma de Madrid, Madrid 28049, Spain
[4]SUPA, School of Physics and Astronomy, University of St Andrews, St. Andrews KY16 9SS, United Kingdom

(Received 15 July 2018; revised manuscript received 19 September 2018; published 26 December 2019)

We theoretically investigate the many-body states of exciton polaritons that can be observed by pump-probe spectroscopy in high-Q inorganic microcavities. Here, a weak-probe "spin-down" polariton is introduced into a coherent state of "spin-up" polaritons created by a strong pump. We show that the $\downarrow$ impurities become dressed by excitations of the $\uparrow$ medium, and that they form new polaronic quasiparticles that feature two-point and three-point many-body quantum correlations that, in the low density regime, arise from coupling to the vacuum biexciton and triexciton states, respectively. In particular, we find that these correlations generate additional branches and avoided crossings in the $\downarrow$ optical transmission spectrum that have a characteristic dependence on the $\uparrow$-polariton density. Our results thus demonstrate a way to directly observe correlated many-body states in an exciton-polariton system that go beyond classical mean-field theories.

DOI: 10.1103/PhysRevLett.123.266401

Although the existence of Bose-Einstein statistics is fundamentally quantum, many of the properties of Bose-Einstein condensates can be understood from the phenomenology of nonlinear classical waves (see, e.g., Ref. [1]). In particular, the physics of a weakly interacting gas at low temperatures can generally be described by mean-field theories involving coherent (i.e., semiclassical) states. Exceptions to this arise when the strength of interactions becomes comparable to the kinetic energy of the bosons. Here, one has correlated states and even quantum phase transitions, e.g., between superfluid and Mott insulating phases [2,3]. For condensates composed of short-lived bosonic particles such as magnons [4], photons [5], and exciton polaritons (superpositions of excitons and cavity photons) [6], the possibility of realizing correlated states suffers a further restriction: the interaction energy scale must exceed the lifetime broadening of the system's quasiparticles. For these reasons, observing quantum correlated many-body states with such quasiparticles remains a challenging goal.

In this Letter, we propose to engineer and probe quantum correlations in a many-body polariton system through quantum impurity physics. Here, a mobile impurity is dressed by excitations of a quantum-mechanical medium, thus forming a new quasiparticle or polaronic state [7,8] that typically defies a mean-field description. Quantum impurity problems have been studied extensively with cold atoms, where one can explore both Bose [9–11] and Fermi [12–18] polarons (corresponding to bosonic and fermionic mediums, respectively). These studies have yielded insight into the formation dynamics of quasiparticles [17,19,20], as well as the impact of few-body bound states on the many-body system [21,22]. Furthermore, in the solid-state context, the Fermi-polaron picture has recently led to a better understanding of excitons immersed in an electron gas [23,24], as well as the relation of this to the Fermi-edge singularity [25].

Here, we will investigate the correlated states of exciton polaritons using the Bose polaron, which is naturally realized by macroscopically pumping a polariton state in a given circular polarization ($\uparrow$), and then applying a weak probe of the opposite ($\downarrow$) species (Fig. 1). Indeed, experimental groups have already carried out polarization-resolved pump-probe spectroscopy in the transmission configuration [26,27]. However, such measurements were interpreted in terms of a mean-field coupled-channel model involving the vacuum biexciton state [28], which neglects the possibility of correlated polaronic states. In contrast, by considering a polaronic description of the state, our Letter shows the important role played by multipoint quantum correlations, how the character of the many-body polaronic state depends on density, and the role of the multipolariton continuum in influencing the transmission spectrum.

To model the quantum-impurity scenario, we go beyond mean-field theory and construct impurity $\downarrow$-polariton wave functions that include two- and three-point quantum many-body correlations. Such strong multipoint correlations can be continuously connected to the existence of multibody bound states in vacuum, namely, $\downarrow\uparrow$ biexcitons

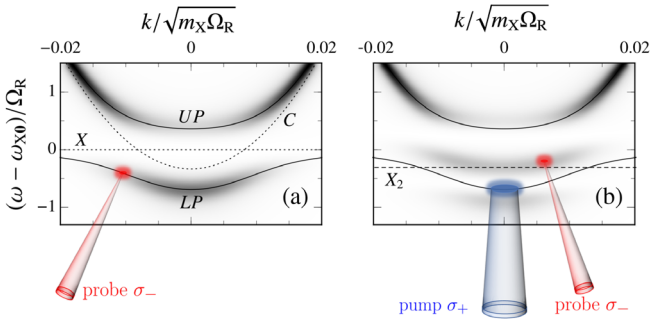

FIG. 1. Spectroscopic signature of a two-point many-body correlated state in the probe photon transmission $\mathcal{T}(\mathbf{k},\omega)$ (see text and [29]) as a function of momentum and energy. (a) In the absence of pumping. The upper polariton (UP) and lower polariton (LP) are shown as solid lines, whereas the dotted lines correspond to the bare photon (C) and exciton (X) dispersions. (b) With a σ_+ pump resonant with the LP at zero momentum. Resonant coupling to a biexciton (X_2) at $\omega + \omega_{\mathrm{LP}0} \simeq -E_B$ (dashed line) causes a splitting of the bare lower polariton into attractive and repulsive branches, as well as a blueshift of the upper polariton. For this illustration, we take the σ_+ polariton density $n = m_X\Omega_R/8\pi$, detuning $\delta = -\Omega_R/3$, and $E_B = \Omega_R$.

and $\downarrow\uparrow\uparrow$ triexcitons [36] (higher-order bound states have not been observed, as far as we are aware). We calculate the $\downarrow$ linear transmission probe spectrum following resonant pumping of $\uparrow$ lower polaritons, as illustrated in Fig. 1(b), and we expose how multipoint correlations emerge as additional splittings in the spectrum with increasing pump strength. There is thus the prospect of directly accessing polariton correlations from spectroscopic measurements performed in standard cryogenic experiments on GaAs-based structures [26,27]—i.e., many-body correlations have measurable effects on transmission measurements, and they do not require measurements of higher-order coherence functions in order to be observed. Moreover, our theory requires few parameters that can be measured independently, and thus allows one to predict the pump-probe spectrum in other materials, such as transition metal dichalcogenides at room temperature [37,38].

Model.—We consider a spin-$\downarrow$ impurity excited by a σ_- probe immersed in a gas of spin-$\uparrow$ lower polaritons excited by a σ_+ pump (see schematic in Fig. 1). The $\downarrow$ probe is optical, but the coupling between $\uparrow$ and $\downarrow$ polarizations arises through the excitonic component. To capture the effect of the medium on this photonic component, it is natural to describe the impurity in terms of excitons ($\hat{b}_{\mathbf{k}}$) with dispersion $\omega_{X\mathbf{k}} = \mathbf{k}^2/2m_X$, and photons ($\hat{c}_{\mathbf{k}}$) with dispersion $\omega_{C\mathbf{k}} = \mathbf{k}^2/2m_C + \delta$. Here, δ is the photon-exciton detuning (we take $\omega_{X\mathbf{0}} = 0$), m_X is the exciton mass, and m_C is the photon mass—in this Letter, we always take $m_C/m_X \simeq 10^{-4}$. The photon-exciton coupling of strength Ω_R leads to the formation of lower and upper exciton polaritons [39,40] with dispersion:

$$\omega^{\mathrm{LP}}_{\mathrm{UP}}{}_{\mathbf{k}} = \frac{1}{2}\left[\omega_{X\mathbf{k}} + \omega_{C\mathbf{k}} \mp \sqrt{(\omega_{C\mathbf{k}} - \omega_{X\mathbf{k}})^2 + \Omega_R^2}\right]. \quad (1)$$

We choose a pump that is resonant with the lower polaritons at zero momentum, yielding a macroscopically occupied single-particle $\mathbf{k} = 0$ state. Thus, we use the following Hamiltonian [29] (setting $\hbar$ and the area to 1):

$$\begin{aligned}\hat{H} = &\sum_{\mathbf{k}}\left(\omega_{X\mathbf{k}}\hat{b}^\dagger_{\mathbf{k}}\hat{b}_{\mathbf{k}} + \omega_{C\mathbf{k}}\hat{c}^\dagger_{\mathbf{k}}\hat{c}_{\mathbf{k}} + \frac{\Omega_R}{2}(\hat{b}^\dagger_{\mathbf{k}}\hat{c}_{\mathbf{k}} + \mathrm{H.c.})\right)\\ &+ \sum_{\mathbf{k}}(\omega_{\mathrm{LP}\mathbf{k}} - \omega_{\mathrm{LP}\mathbf{0}})\hat{L}^\dagger_{\mathbf{k}}\hat{L}_{\mathbf{k}} + \sum_{\mathbf{k},\mathbf{k}',\mathbf{q}} g_{\mathbf{k}\mathbf{k}'}\hat{L}^\dagger_{\mathbf{k}}\hat{b}^\dagger_{\mathbf{q}-\mathbf{k}}\hat{b}_{\mathbf{q}-\mathbf{k}'}\hat{L}_{\mathbf{k}'}\\ &+ \sqrt{n}\sum_{\mathbf{k},\mathbf{q}} g_{\mathbf{k}\mathbf{0}}\hat{b}^\dagger_{\mathbf{q}-\mathbf{k}}\hat{b}_{\mathbf{q}}(\hat{L}^\dagger_{\mathbf{k}} + \hat{L}_{-\mathbf{k}}), \end{aligned} \quad (2)$$

which is measured with respect to the energy of the Bose medium in the absence of excitations, $\omega_{\mathrm{LP}\mathbf{0}}n$, where n is the medium density. Because only the $\uparrow$ LP mode is occupied, we simplify our calculations by writing the medium in the polariton basis with the finite-momentum LP creation operator $\hat{L}^\dagger_{\mathbf{k}}$ and excitation energy $\omega_{\mathrm{LP}\mathbf{k}} - \omega_{\mathrm{LP}\mathbf{0}}$. In order to extract the photon transmission, however, we work with exciton and photon operators for the impurity. For simplicity, we have assumed that the polariton splitting and detuning are independent of polarization; however, it is straightforward to generalize our results to polarization-dependent parameters.

We model the $\uparrow$-$\downarrow$ interactions between excitons using a contact potential that, in momentum space, is constant with strength g up to a momentum cutoff Λ. This is reasonable because typical polariton wavelengths of $\sim 1/\sqrt{m_C\Omega_R}$ greatly exceed the exciton Bohr radius that sets the exciton-exciton interaction length scale [41,42]. The exciton-polariton coupling in Eq. (2) is given by $g_{\mathbf{k}\mathbf{k}'} = g\cos\theta_{\mathbf{k}}\cos\theta_{\mathbf{k}'}$, with the Hopfield factor [39]

$$\cos\theta_{\mathbf{k}} = \frac{1}{\sqrt{2}}\sqrt{1 + \frac{\omega_{C\mathbf{k}} - \omega_{X\mathbf{k}}}{\sqrt{(\omega_{C\mathbf{k}} - \omega_{X\mathbf{k}})^2 + \Omega_R^2}}}, \quad (3)$$

which corresponds to (the square root of) the exciton fraction in the LP state at a given momentum. As is standard in two-dimensional quantum gases (see, e.g., Ref. [43]), the coupling constant and cutoff are related to the biexciton binding energy E_B (which we define as positive) through the process of renormalization:

$$-\frac{1}{g} = \sum_{\mathbf{k}}^{k<\Lambda}\frac{1}{E_B + 2\omega_{X\mathbf{k}}} = \frac{m_X}{4\pi}\ln\left(\frac{\Lambda^2/m_X + E_B}{E_B}\right). \quad (4)$$

This treatment of the ultraviolet physics is justified as long as the biexciton size greatly exceeds that of the exciton, which is the case when the masses of the electron and the hole making up the exciton are comparable [44].

We neglect interactions in the medium for simplicity—in the Supplemental Material [29], we show that adding interactions in the medium does not significantly change the results.

Probe photon transmission.—The transmission $\mathcal{T}(\mathbf{k},\omega)$ of a photon at frequency ω and momentum $\mathbf{k}$ is related to the photon retarded Green's function [45] via $\mathcal{T}(\mathbf{k},\omega) = |G_C(\mathbf{k},\omega)|^2$, where we ignore a constant prefactor that only depends on the loss rate through the mirrors. To evaluate this, we note that only the exciton component of the impurity interacts with the medium. Then, in the exciton-photon basis, the impurity Green's function has the form of a matrix,

$$\mathbf{G}(\mathbf{k},\omega) = \begin{pmatrix} G_X^{(0)}(\mathbf{k},\omega)^{-1} - \Sigma_X(\mathbf{k},\omega) & -\Omega_R/2 \\ -\Omega_R/2 & G_C^{(0)}(\mathbf{k},\omega)^{-1} \end{pmatrix}^{-1}, \tag{5}$$

where $G_C \equiv \mathbf{G}_{22}$. Here, the exciton and photon Green's functions in the absence of interactions are $G_{X,C}^{(0)}(\mathbf{k},\omega) = 1/(\omega - \omega_{X,C\mathbf{k}} + i0)$, respectively, where the frequency poles are shifted infinitesimally into the lower complex plane. Importantly, Eq. (5) is an exact relation within the Hamiltonian [Eq. (2)], which highlights how any approximation to the probe transmission arises from the calculation of the exciton self-energy Σ_X.

In the following, we evaluate the photon Green's function by using the truncated basis method (TBM) [19]. Within this approximation, the Hilbert space of impurity wave functions is restricted to describe only a finite number of excitations of the medium. The Green's function can be found (as will be discussed below) by summing over all eigenstates in this basis. In the context of ultracold gases, such an approximation has been shown to successfully reproduce the experimentally observed spectral function of impurities immersed in a Bose-Einstein condensate [10], as well as the ground state [46,47] and coherent quantum dynamics of impurities in a Fermi sea [17]. As such, the TBM is an appropriate approximation for the investigation of impurity physics, both in and out of equilibrium. Note further that the TBM in principle allows us to investigate other dynamical observables [19], such as higher-order coherence functions [48].

Impurity wave function.—To capture the signatures of strong two- and three-point correlations in the probe transmission, we introduce a variational wave function containing terms where the impurity is dressed by up to two excitations of the medium:

$$|\Psi\rangle = \left(\gamma_0\hat{c}_{\mathbf{0}}^\dagger + \alpha_0\hat{b}_{\mathbf{0}}^\dagger + \sum_{\mathbf{k}}\alpha_{\mathbf{k}}\hat{b}_{-\mathbf{k}}^\dagger\hat{L}_{\mathbf{k}}^\dagger + \frac{1}{2}\sum_{\mathbf{k}_1\mathbf{k}_2}\alpha_{\mathbf{k}_1\mathbf{k}_2}\hat{b}_{-\mathbf{k}_1-\mathbf{k}_2}^\dagger\hat{L}_{\mathbf{k}_1}^\dagger\hat{L}_{\mathbf{k}_2}^\dagger\right)|\Phi\rangle. \tag{6}$$

Here, $|\Phi\rangle$ is the coherent state describing the medium in the absence of the impurity, and we consider a σ_- probe at normal incidence, where the total momentum imparted is zero. We take advantage of the fact that the large mass difference between photons and excitons acts to suppress terms in the wave function containing impurity photons at finite momentum—i.e., terms such as $\gamma_{\mathbf{k}}\hat{c}_{-\mathbf{k}}^\dagger\hat{L}_{\mathbf{k}}^\dagger$ and $\gamma_{\mathbf{k}_1\mathbf{k}_2}\hat{c}_{-\mathbf{k}_1-\mathbf{k}_2}^\dagger\hat{L}_{\mathbf{k}_1}^\dagger\hat{L}_{\mathbf{k}_2}^\dagger$ are far detuned in energy from the other terms in the wave function, and have thus been neglected. We then find the impurity spectrum by solving $\hat{H}|\Psi\rangle = E|\Psi\rangle$ within the truncated Hilbert space given by wave functions of the form in Eq. (6). This procedure yields a set of coupled linear equations that we solve numerically [29].

Within the TBM, once all eigenvalues and vectors of the linear equations are known, the photon Green's function can be written as [29]

$$G_C(\mathbf{0},\omega) \simeq \sum_n \frac{|\gamma_0^{(n)}|^2}{\omega - E_n + i\Gamma}. \tag{7}$$

The sum runs over all eigenstates within the truncated Hilbert space, picking out the weight of the photon term from each. The factor $i\Gamma$ introduces broadening because of microcavity finite lifetime effects. For simplicity, we take it to be independent of the state, which corresponds to considering equal exciton and photon lifetimes. This does not qualitatively affect the results of our work.

Results.—In Fig. 2, we show our calculated normal incidence pump-probe transmission as a function of the photon-exciton detuning and the probe frequency. In the limit of vanishing pump power [Fig. 2(a)], the probe transmission is given by the single-particle LP and UP branches as expected [39,40], with the relative weights varying according to the photonic fraction of each branch. On increasing the pump strength, we observe first one and then two additional branches appearing with clear avoided crossings, as depicted in Figs. 2(b) and 2(c). This happens in the vicinity of where the LP and UP branches become resonant with either a biexciton (X_2) or a triexciton (X_3) state: Indeed, recalling that we set the $k = 0$ exciton energy to zero, the crossings between solid and dashed lines correspond to the zero-density resonance conditions $\omega^* + \omega_{\mathrm{LP}\mathbf{0}} = -E_B$ and $\omega^* + 2\omega_{\mathrm{LP}\mathbf{0}} = \varepsilon_T$, where ε_T is the vacuum triexciton energy, and $\omega^* \in \{\omega_{\mathrm{LP}\mathbf{0}}, \omega_{\mathrm{UP}\mathbf{0}}\}$. The resonant behavior results in an intriguing transmission spectrum, where both lower and upper polaritons split into red-shifted attractive and blue-shifted repulsive polaronic quasiparticle branches due to the X_3 and X_2 resonances. Furthermore, at sufficiently large densities, we see that the two LP repulsive branches smoothly evolve into the corresponding attractive and repulsive branches of the UP state.

It is important to distinguish the nature of the polaron state we describe here from the mean-field coupled-channel

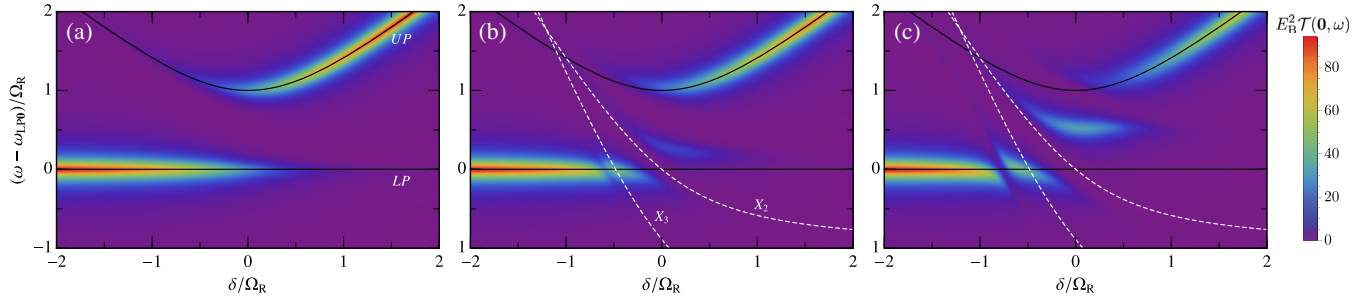

FIG. 2. Normal incidence pump-probe transmission $\mathcal{T}(\mathbf{0},\omega)$ as a function of the photon-exciton detuning and the rescaled probe energy (relative to the LP energy) for increasing pump densities: (a) $n=0$, (b) $n=m_X\Omega_R/16\pi$, and (c) $n=m_X\Omega_R/4\pi$. In the experimentally realistic case of $\Omega_R=3$ meV, this corresponds to densities of (b) $n=3\times10^{10}$ cm^{-2} and (c) $n=1.25\times10^{11}$ cm^{-2}. In both cases, we take $E_B=\Omega_R$ and a broadening of $\Gamma=\Omega_R/10$. Lower and upper polariton energies in the absence of the medium are shown as black solid lines. Dashed white lines indicate locations of the vacuum biexciton (X_2) and triexciton (X_3) resonances at $\omega+\omega_{\mathrm{LP0}}=-E_B$ and $\omega+2\omega_{\mathrm{LP0}}=\varepsilon_T$, respectively, with triexciton energy of $\varepsilon_T\simeq-2.4E_B$ [29].

picture described elsewhere [26,27] that, at low densities, produces a qualitatively similar spectrum. In the coupled-channel model, there is an anticrossing between the polariton branches and a preformed molecular state. By contrast, the X_2 splitting described in this Letter is a beyond-mean-field many-body effect due to two-point correlations that are enhanced by the biexciton resonance. Similarly, the appearance of additional branches at higher densities demonstrates the emergence of many-body three-point correlated states. Indeed, we see that the X_3 resonance position gets rapidly shifted from the vacuum triexciton energy when increasing the density, due to the influence of the continuum of unbound polariton states at high energies; see [29]. Note that our model is likely to overestimate the magnitude of the triexciton energy $|\varepsilon_T|$ because we have neglected the repulsion between $\uparrow$ excitons. However, we can show that the triexciton remains bound even when there is an effective three-body repulsion (which mimics the $\uparrow$-$\uparrow$ repulsion [22]), and the triexciton binding energy only weakly depends on this repulsion [29].

In order to quantify the density dependence of the two X_2 and X_3 resonances for the lower polariton, we evaluate in Fig. 3 the minimal splittings $\Delta\omega_{2,3}$ between repulsive and attractive branches and the corresponding detunings $\delta_{2,3}$ at which these anticrossings occur when the finite lifetime broadening Γ can be neglected [29]. In the low-density limit, one can formally show that the minimal splitting due to the X_2 resonance has the form $\Delta\omega_2\sim\cos\theta_0\sqrt{nE_B/m_X}$ [29]. This behavior is captured using two-point correlations only; indeed, we see in Fig. 3(a) that two-point correlations dominate even at higher densities. However, the shift in the detuning δ_2 is a higher-order density effect that can be affected by three-point correlations, as illustrated in Fig. 3(b). For the X_3 resonance, the splitting $\Delta\omega_3$ shown in Fig. 3(a) approaches a linear scaling with n as $n\to0$. In this case, one can show that the energy shift of the attractive branch scales linearly with n at low densities, whereas the repulsive branch only shifts upwards once δ_3 moves away from the vacuum resonance position [29]. Note that, in the presence of broadening, a given splitting $\Delta\omega$ is only visible when $\Delta\omega\gtrsim\Gamma$.

Implications for experiments.—As previously mentioned, the pump-probe protocol employed in the experiments by Takemura *et al.* [26,27] is similar to our impurity scenario. However, Ref. [27] had a large broadening Γ so that the splitting could not be resolved, whereas the experiment of Ref. [26] employed a broad pump that populated both $\uparrow$ LP and UP branches. Nevertheless, if we take $\Omega_R=E_B=3$ meV, then the parameters chosen for Fig. 2(c) correspond to a density of $n=1.25\times10^{11}$ cm^{-2}, which approximately matches the parameters of figure 3 in Ref. [26]. Here, the splitting of the lower polariton close to the biexciton resonance was analyzed [26]. Qualitatively, our results for the attractive and repulsive energy shifts

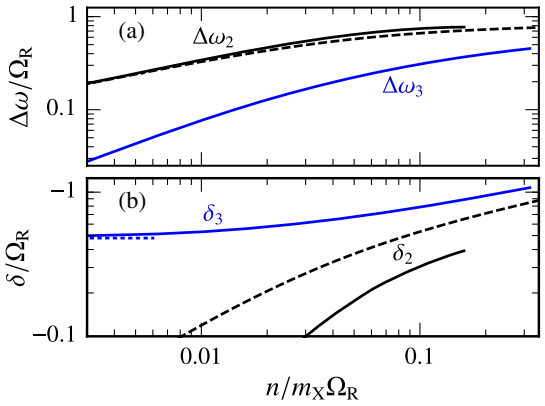

FIG. 3. (a) Minimal splitting between LP quasiparticle branches in the transmission spectrum, and (b) photon-exciton detuning at the minimal splitting. The splitting $\Delta\omega_3$ and the detuning δ_3 for the lowest two branches—originating from the triexciton resonance—are shown as solid blue lines, where $\delta_3\to-0.48\Omega_R$ (dotted line) is the limit $n\to0$ due to the triexciton state. Splitting $\Delta\omega_2$ and detuning δ_2 for the biexciton resonance are shown as solid black lines. Dashed black lines depict corresponding results calculated when including only two-point correlations (i.e., the Hilbert space with, at most, one excitation of the medium).

agree; however the measured energy shifts are somewhat smaller than what we find. This is likely to be due to the broad range of ↑ states populated in Ref. [26], which will tend to wash out the effect of the resonances as compared to when the bosonic medium is a macroscopically occupied single-particle state.

Conclusions and outlook.—In this Letter, we have shown how many-body correlations in the exciton-polariton system can be directly accessed using pump-probe spectroscopy. Such measurements are complementary to the sophisticated multidimensional optical spectroscopy techniques employed in, e.g., Ref. [49], which required multiple phase-stable optical pulses with controllable delays. Furthermore, depending on the material parameters, there is even the possibility of overlapping biexciton and triexciton resonances, where both two- and three-point correlations are enhanced [29]. Direct probes of the many-body correlated states can also provide stringent bounds on the nature and spin structure of the polariton-polariton interaction. Such an approach is complementary to measurements of the blueshift (which can be affected by reservoir excitons) and is crucial in the progress towards realizing truly quantum states. Recently, there has been significant interest and some progress toward achieving antibunching in emission from fully confined photonic dots [50,51]. However, there is as yet little known about many-body correlated polariton states. Our results suggest that exploring impurity physics in polariton condensates provides a route to achieve this.

The research data underpinning this publication can be accessed at [52].

We are grateful to A. İmamoğlu for useful discussions. J. L. and M. M. P. acknowledge support from the Australian Research Council Centre of Excellence in Future Low-Energy Electronics Technologies (CE170100039). J. L. is also supported through the Australian Research Council Future Fellowship FT160100244. F. M. M. acknowledges financial support from the Ministerio de Economía y Competitividad, Projects No. MAT2014-53119-C2-1-R and No. MAT2017-83772-R. J. K. acknowledges financial support from the EPSRC program "Hybrid Polaritonics" (EP/M025330/1). This work was performed in part at the Aspen Center for Physics, which is supported by the National Science Foundation by Grant No. PHY-1607611. This work was partially supported by a grant from the Simons Foundation.

[1] N. Proukakis, S. Gardiner, M. Davis, and M. Szymańska, *Quantum Gases* (Imperial College Press, London, 2013).

[2] M. Greiner, O. Mandel, T. Esslinger, T. W. Hänsch, and I. Bloch, Quantum phase transition from a superfluid to a Mott insulator in a gas of ultracold atoms, Nature (London) **415**, 39 (2002).

[3] I. Bloch, J. Dalibard, and W. Zwerger, Many-body physics with ultracold gases, Rev. Mod. Phys. **80**, 885 (2008).

[4] S. O. Demokritov, V. E. Demidov, O. Dzyapko, G. A. Melkov, A. A. Serga, B. Hillebrands, and A. N. Slavin, Bose–Einstein condensation of quasi-equilibrium magnons at room temperature under pumping, Nature (London) **443**, 430 (2006).

[5] J. Klaers, J. Schmitt, F. Vewinger, and M. Weitz, Bose-Einstein condensation of photons in an optical microcavity, Nature (London) **468**, 545 (2010).

[6] J. Kasprzak, M. Richard, S. Kundermann, A. Baas, P. Jeambrun, J. M. J. Keeling, F. M. Marchetti, M. H. Szymańska, R. André, J. L. Staehli, V. Savona, P. B. Littlewood, B. Deveaud, and L. S. Dang, Bose-Einstein condensation of exciton polaritons, Nature (London) **443**, 409 (2006).

[7] G. Mahan, *Many-Particle Physics*, Physics of Solids and Liquids (Springer, New York, 2013).

[8] J. T. Devreese and A. S. Alexandrov, Fröhlich polaron and bipolaron: Recent developments, Rep. Prog. Phys. **72**, 066501 (2009).

[9] M. G. Hu, M. J. Van De Graaff, D. Kedar, J. P. Corson, E. A. Cornell, and D. S. Jin, Bose Polarons in the Strongly Interacting Regime, Phys. Rev. Lett. **117**, 055301 (2016).

[10] N. B. Jørgensen, L. Wacker, K. T. Skalmstang, M. M. Parish, J. Levinsen, R. S. Christensen, G. M. Bruun, and J. J. Arlt, Observation of Attractive and Repulsive Polarons in a Bose-Einstein Condensate, Phys. Rev. Lett. **117**, 055302 (2016).

[11] F. Camargo, R. Schmidt, J. D. Whalen, R. Ding, G. Woehl, S. Yoshida, J. Burgdörfer, F. B. Dunning, H. R. Sadeghpour, E. Demler, and T. C. Killian, Creation of Rydberg Polarons in a Bose Gas, Phys. Rev. Lett. **120**, 083401 (2018).

[12] A. Schirotzek, C.-H. Wu, A. Sommer, and M. W. Zwierlein, Observation of Fermi Polarons in a Tunable Fermi Liquid of Ultracold Atoms, Phys. Rev. Lett. **102**, 230402 (2009).

[13] S. Nascimbène, N. Navon, K. J. Jiang, L. Tarruell, M. Teichmann, J. McKeever, F. Chevy, and C. Salomon, Collective Oscillations of an Imbalanced Fermi Gas: Axial Compression Modes and Polaron Effective Mass, Phys. Rev. Lett. **103**, 170402 (2009).

[14] C. Kohstall, M. Zaccanti, M. Jag, A. Trenkwalder, P. Massignan, G. M. Bruun, F. Schreck, and R. Grimm, Metastability and coherence of repulsive polarons in a strongly interacting Fermi mixture, Nature (London) **485**, 615 (2012).

[15] M. Koschorreck, D. Pertot, E. Vogt, B. Fröhlich, M. Feld, and M. Köhl, Attractive and repulsive Fermi polarons in two dimensions, Nature (London) **485**, 619 (2012).

[16] M. Cetina, M. Jag, R. S. Lous, J. T. M. Walraven, R. Grimm, R. S. Christensen, and G. M. Bruun, Decoherence of Impurities in a Fermi Sea of Ultracold Atoms, Phys. Rev. Lett. **115**, 135302 (2015).

[17] M. Cetina, M. Jag, R. S. Lous, I. Fritsche, J. T. M. Walraven, R. Grimm, J. Levinsen, M. M. Parish, R. Schmidt, M. Knap, and E. Demler, Ultrafast many-body interferometry of impurities coupled to a Fermi sea, Science **354**, 96 (2016).

[18] F. Scazza, G. Valtolina, P. Massignan, A. Recati, A. Amico, A. Burchianti, C. Fort, M. Inguscio, M. Zaccanti, and

G. Roati, Repulsive Fermi Polarons in a Resonant Mixture of Ultracold ^{6}Li Atoms, Phys. Rev. Lett. **118**, 083602 (2017).
[19] M. M. Parish and J. Levinsen, Quantum dynamics of impurities coupled to a Fermi sea, Phys. Rev. B **94**, 184303 (2016).
[20] Y. E. Shchadilova, R. Schmidt, F. Grusdt, and E. Demler, Quantum Dynamics of Ultracold Bose Polarons, Phys. Rev. Lett. **117**, 113002 (2016).
[21] P. Massignan, M. Zaccanti, and G. M. Bruun, Polarons, dressed molecules and itinerant ferromagnetism in ultracold Fermi gases, Rep. Prog. Phys. **77**, 034401 (2014).
[22] S. M. Yoshida, S. Endo, J. Levinsen, and M. M. Parish, Universality of an Impurity in a Bose-Einstein Condensate, Phys. Rev. X **8**, 011024 (2018).
[23] M. Sidler, P. Back, O. Cotlet, A. Srivastava, T. Fink, M. Kroner, E. Demler, and A. Imamoglu, Fermi polaron-polaritons in charge-tunable atomically thin semiconductors, Nat. Phys. **13**, 255 (2017).
[24] D. K. Efimkin and A. H. MacDonald, Many-body theory of trion absorption features in two-dimensional semiconductors, Phys. Rev. B **95**, 035417 (2017).
[25] D. Pimenov, J. von Delft, L. Glazman, and M. Goldstein, Fermi-edge exciton-polaritons in doped semiconductor microcavities with finite hole mass, Phys. Rev. B **96**, 155310 (2017).
[26] N. Takemura, S. Trebaol, M. Wouters, M. T. Portella-Oberli, and B. Deveaud, Polaritonic Feshbach resonance, Nat. Phys. **10**, 500 (2014).
[27] N. Takemura, M. D. Anderson, M. Navadeh-Toupchi, D. Y. Oberli, M. T. Portella-Oberli, and B. Deveaud, Spin anisotropic interactions of lower polaritons in the vicinity of polaritonic Feshbach resonance, Phys. Rev. B **95**, 205303 (2017).
[28] M. Wouters, Resonant polariton-polariton scattering in semiconductor microcavities, Phys. Rev. B **76**, 045319 (2007).
[29] See Supplemental Material at http://link.aps.org/supplemental/10.1103/PhysRevLett.123.266401 for details on the model, the TBM equations including interactions in the medium, and the equations for the three-body bound state. This includes references to [30–35].
[30] L. W. Bruch and J. A. Tjon, Binding of three identical bosons in two dimensions, Phys. Rev. A **19**, 425 (1979).
[31] I. Carusotto and C. Ciuti, Quantum fluids of light, Rev. Mod. Phys. **85**, 299 (2013).
[32] J. Levinsen, M. M. Parish, and G. M. Bruun, Impurity in a Bose-Einstein Condensate and the Efimov Effect, Phys. Rev. Lett. **115**, 125302 (2015).
[33] F. Tassone and Y. Yamamoto, Exciton-exciton scattering dynamics in a semiconductor microcavity and stimulated scattering into polaritons, Phys. Rev. B **59**, 10830 (1999).
[34] M. Wouters and I. Carusotto, Excitations in a Nonequilibrium Bose-Einstein Condensate of Exciton Polaritons, Phys. Rev. Lett. **99**, 140402 (2007).
[35] I. Carusotto and C. Ciuti, Probing Microcavity Polariton Superfluidity Through Resonant Rayleigh Scattering, Phys. Rev. Lett. **93**, 166401 (2004).
[36] D. B. Turner and K. A. Nelson, Coherent measurements of high-order electronic correlations in quantum wells, Nature (London) **466**, 1089 (2010).
[37] L. C. Flatten, Z. He, D. M. Coles, A. A. Trichet, A. W. Powell, R. A. Taylor, J. H. Warner, and J. M. Smith, Room-temperature exciton-polaritons with two-dimensional WS 2, Sci. Rep. **6**, 33134 (2016).
[38] N. Lundt, S. Klembt, E. Cherotchenko, S. Betzold, O. Iff, A. V. Nalitov, M. Klaas, C. P. Dietrich, A. V. Kavokin, S. Höfling *et al.*, Room-temperature Tamm-plasmon exciton-polaritons with a WSe 2 monolayer, Nat. Commun. **7**, 13328 (2016).
[39] J. J. Hopfield, Theory of the contribution of excitons to the complex dielectric constant of crystals, Phys. Rev. **112**, 1555 (1958).
[40] S. Pekar, The theory of electromagnetic waves in a crystal in which excitons are produced, Zh. Eksp. Teor. Fiz. **33**, 1022 (1958) [JETP **6**, 785 (1958)].
[41] C. Ciuti, V. Savona, C. Piermarocchi, A. Quattropani, and P. Schwendimann, Role of the exchange of carriers in elastic exciton-exciton scattering in quantum wells, Phys. Rev. B **58**, 7926 (1998).
[42] G. Rochat, C. Ciuti, V. Savona, C. Piermarocchi, A. Quattropani, and P. Schwendimann, Excitonic Bloch equations for a two-dimensional system of interacting excitons, Phys. Rev. B **61**, 13856 (2000).
[43] J. Levinsen and M. M. Parish, Strongly interacting two-dimensional Fermi gases, Annu. Rev. Cold At. Mol. **3**, 1 (2015).
[44] A. Ivanov, H. Haug, and L. Keldysh, Optics of excitonic molecules in semiconductors and semiconductor microstructures, Phys. Rep. **296**, 237 (1998).
[45] C. Ciuti and I. Carusotto, Input-output theory of cavities in the ultrastrong coupling regime: The case of time-independent cavity parameters, Phys. Rev. A **74**, 033811 (2006).
[46] F. Chevy, Universal phase diagram of a strongly interacting Fermi gas with unbalanced spin populations, Phys. Rev. A **74**, 063628 (2006).
[47] J. Vlietinck, J. Ryckebusch, and K. Van Houcke, Quasiparticle properties of an impurity in a Fermi gas, Phys. Rev. B **87**, 115133 (2013).
[48] M. Klaas, H. Flayac, M. Amthor, I. G. Savenko, S. Brodbeck, T. Ala-Nissila, S. Klembt, C. Schneider, and S. Höfling, Evolution of Temporal Coherence in Confined Exciton-Polariton Condensates, Phys. Rev. Lett. **120**, 017401 (2018).
[49] P. Wen, G. Christmann, J. J. Baumberg, and K. A. Nelson, Influence of multi-exciton correlations on nonlinear polariton dynamics in semiconductor microcavities, New J. Phys. **15**, 025005 (2013).
[50] G. Muñoz-Matutano, A. Wood, M. Johnsson, X. Vidal, B. Q. Baragiola, A. Reinhard, A. Lemaître, J. Bloch, A. Amo, G. Nogues, B. Besga, M. Richard, and T. Volz, Emergence of quantum correlations from interacting fibre-cavity polaritons, Nat. Mater. **18**, 213 (2019).
[51] A. Delteil, T. Fink, A. Schade, S. Höfling, C. Schneider, and A. İmamoğlu, Towards polariton blockade of confined exciton–polaritons, Nat. Mater. **18**, 219 (2019).
[52] J. Levinsen, F. M. Marchetti, J. M. J. Keeling, and M. Parish, Data Underpinning: Spectroscopic probes of quantum many-body correlations in polariton microcavities. Dataset. University of St Andrews Research Portal, https://doi.org/10.17630/68007109-18b9-46ca-95a1-5cbcb173b4d0 (2019).